Implications of Mini-EUSO measurements for a space-based observation of UHECRs

Mario Bertaina[a,*] **and Matteo Battisti**[b] **for the JEM-EUSO Collaboration**

(a complete list of authors can be found at the end of the proceedings)

[a]*Università di Torino & INFN Sezione di Torino,*

[b]*INFN sezione di Roma Tor Vergata,*

E-mail: bertaina@to.infn.it

Mini–EUSO (Multiwavelength Imaging New Instrument for the Extreme Universe Space Observatory, known as *UV atmosphere* in the Russian Space Program) is the first mission of the JEM-EUSO program on board the International Space Station. It was launched in August 2019 and it is operating since October 2019 being located in the Russian section (Zvezda module) of the station and viewing our planet from a nadir-facing UV-transparent window. The instrument is based on the concept of the original JEM-EUSO mission and consists of an optical system employing two Fresnel lenses of 25 cm each and a focal surface composed of 36 Multi-Anode Photomultiplier tubes, 64 channels each, for a total of 2304 channels with single photon counting sensitivity and an overall field of view of 44°×44°. Mini-EUSO can map the night-time Earth in the near UV range (predominantly between 290 nm and 430 nm), with a spatial resolution of about 6 km and different temporal resolutions of 2.5 μs, 320 μs and 41 ms. Mini-EUSO observations are extremely important to better assess the potential of a space-based detector in studying Ultra-High Energy Cosmic Rays (UHECRs) such as K-EUSO and POEMMA. In this contribution we focus the attention on the results of the UV measurements and we place them in the context of UHECR observations from space, namely the estimation of exposure for the planned M-EUSO (Multi-messenger Extreme Universe Space Observatory) mission.

---

*Speaker

1. Introduction

The current main goal in the field of UHECR (Ultra-High Energy Cosmic Ray) science is to identify their astrophysical sources and acceleration mechanisms [1]. For this, increased statistics at the highest energies is one of the essential requirements. A space-based detector for UHECR research has the advantage of a very large exposure and a uniform coverage of the celestial sphere. The aim of the JEM-EUSO program [2] is to bring the study of UHECRs to space. The principle of observation is based on the detection of UV light emitted by isotropic fluorescence of atmospheric nitrogen excited by Extensive Air Showers (EASs) in Earth's atmosphere and forward-beamed Cherenkov radiation reflected at the Earth's surface or at dense cloud tops.

The JEM-EUSO program includes missions on ground (EUSO-TA [3]), on stratospheric balloons (EUSO-Balloon [4], EUSO-SPB1 [5], EUSO-SPB2 [6], PBR [7]), and from space (TUS [8], Mini-EUSO [9]) employing fluorescence detectors to demonstrate the feasibility of the UHECR observation from space and prepare for the large size missions K-EUSO [10], POEMMA [11] and the currently proposed M-EUSO mission [2] in response to the M8 ESA call of spring 2025.

Mini-EUSO is the first detector of the JEM-EUSO program to observe the Earth from the International Space Station (ISS) and to validate from there the observational principle of a space-based detector for UHECR measurements. This means primarily demonstrating that a space-based observatory has a sufficiently high duty cycle, meant as the fraction of time in which the atmospheric or anthropogenic light sources do not prevent the observation of a UHECR from space, as well as the capability to detect short light transients which show similarities in terms of either the light intensity or pulse duration with what is expected from an EAS cascading in the atmosphere.

2. The Mini-EUSO instrument and operation

Mini–EUSO [9] is a telescope operating in the near UV range, predominantly between 290 nm and 430 nm, with a square focal surface corresponding to a field of view (FoV) of ~44° × 44°. Its spatial resolution at ground level is ~6×6 km^2, slightly varying with the altitude of the ISS and the pointing direction of the pixel. The detector size is $37 \times 37 \times 62$ cm^3, mainly constrained by the size of the nadir-facing UV transparent window in the Russian Zvezda module. Until April 2025 more than 150 sessions have been successfully performed. Currently, only the first 44 sessions are fully available for analysis. However, the remaining data up to April 2025 have been downloaded to ground and will be soon ready as well.

The optics are based on two 25 cm diameter Fresnel lenses in Polymethyl methacrylate (PMMA). The Mini–EUSO focal surface, or Photo Detection Module (PDM), consists of a grid of 36 Multi-Anode Photomultiplier Tubes (MAPMTs) arranged in an array of 6×6 elements. Each MAPMT consists of 8×8 pixels, resulting in a total of 2304 channels. The system collects data with three different time resolutions at the same time. The 2.5 μs GTU data stream (D1) is saved in a running buffer on which the trigger code is executed (further details in [12]). Similarly, an independent data stream with a dedicated trigger system and a time resolution of 320μs (D2) is present. Finally, the longest time resolution of 40.96 ms (D3) is continuously stored. An end-to-end in-flight calibration of the detector has been performed by assembling different UV-flasher systems on ground in Japan, Italy, and France and by firing them in various observational campaigns [13]. It

2

made use of a flasher system consisting of a calibrated array of nine 100W COB-UV LEDs, batteries and an Arduino circuit. In 2022, an observational campaign was performed at Sant'Antimo Abbey (Italy) at the altitude of ~320 m a.s.l. The place was chosen based on the very low light pollution in an area of several km radius. Photons from the UV flasher were detected and the overall efficiency of Mini-EUSO was estimated to be $\epsilon_{ME} = 0.061 \pm 0.020$ at $\lambda = 400$ nm.[1]

3. Typical background variability during an orbit of Mini-EUSO

Mini-EUSO has been designed to detect a photon rate per pixel from diffuse sources (nightglow, clouds, cities, etc.) in the range of values expected from a large mission in space such as the original JEM-EUSO mission [14]. The pixel FoV is, therefore, ~100 times larger in area with respect to the FoV of a JEM-EUSO pixel (0.5 km × 0.5 km), to compensate for the optical system ~100 times smaller, constrained by the dimension of the UV transparent window where Mini-EUSO is installed during the data taking sessions. As a consequence, the energy threshold of Mini-EUSO for UHECRs is well above 10^{21} eV (see Fig. 1).
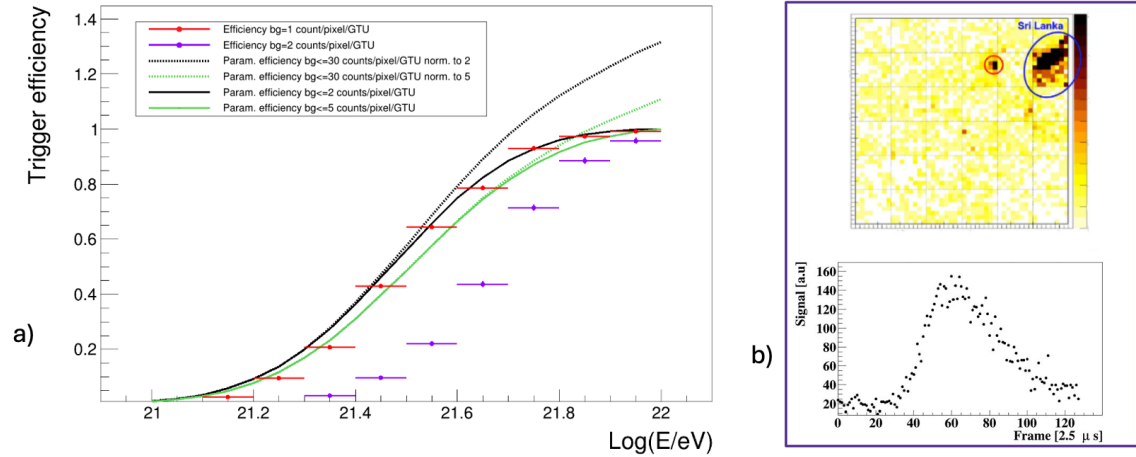

Figure 1: a) The figure shows the trigger efficiency of Mini-EUSO as a function of energy for different background conditions (see Sect. 4 for details). b) Image (top) and light profile (down) of a Short Light Transients detected by Mini-EUSO near Sri Lanka. The event has duration and light intensity similar to what is expected from an EAS signal even though their kinematics do not match (see discussion on Sect. 4).

Fig. 2 shows a portion of Mini-EUSO orbit on Session 30, which took place on January 9th 2021 around 7:30 UTC. It displays an example of the different conditions that Mini-EUSO observes during an orbit: clear sky, cloudy conditions, city lights and land. Image a) shows the UV map as a function of longitude and latitude. The counts/pix/GTU are color coded in image b). They have been taken in D3 mode but normalized to the D1 GTU. Plot c) displays the light curve along the orbit of one pixel of Mini-EUSO. Plot d) presents the map of artificial lights in US and Canada [15] where the intensity is expressed in fractions above natural light intensity, while e) the atmospheric conditions during the passage over ocean by means of a post-processing analysis of the weather

---

[1]Typically, Mini-EUSO data are equalized through the use of a flat field map, to remove the differences in efficiency among the pixels. This value represents the efficiency of the flat fielded data.

forecast obtained with the data collected by the Global Forecast System (GFS) [16]. The orbit of Mini-EUSO is highlighted by the three lines indicating the center and edges of the FoV of Mini-EUSO. As expected the lowest counts are detected over ocean on clear atmospheric conditions. In the presence of clouds the counts increase and the color contour matches in general the shape of the cloud location. The city lights of Hawaii islands are clearly visible in both a) (yellow spot) and c) (sharp peak increase of light). The presence of thunderstorm activity in the cloudy area between 7h36 and 7h39 UTC can be deduced by the pixel data reported in c) which show rapid increase and decrease of photon counts. Before entering the US coast there is a less cloudy region and the counts tend to decrease. Afterwards, when entering the US west coast sudden peaks in photon counts are observed. They are due to the passage on particularly bright areas as depicted in map d). The counts remain higher than over the ocean also in the much less urbanized areas of Canada. This is due to the presence of snow which is highly reflective. The slightly higher counts on the St. Lawrence Bay in Quebec are due to the presence of low clouds. When Mini-EUSO goes back over the ocean the light intensity decreases again to ocean levels. The final sudden increase of counts is due to the sunrise which ends the night time of the orbit. This example shows the capability of the UV camera of Mini-EUSO to infer autonomously different atmospheric or ground scenarios encountered during the flight. Mini-EUSO results on the average UV emissions in different conditions: clear and cloudy
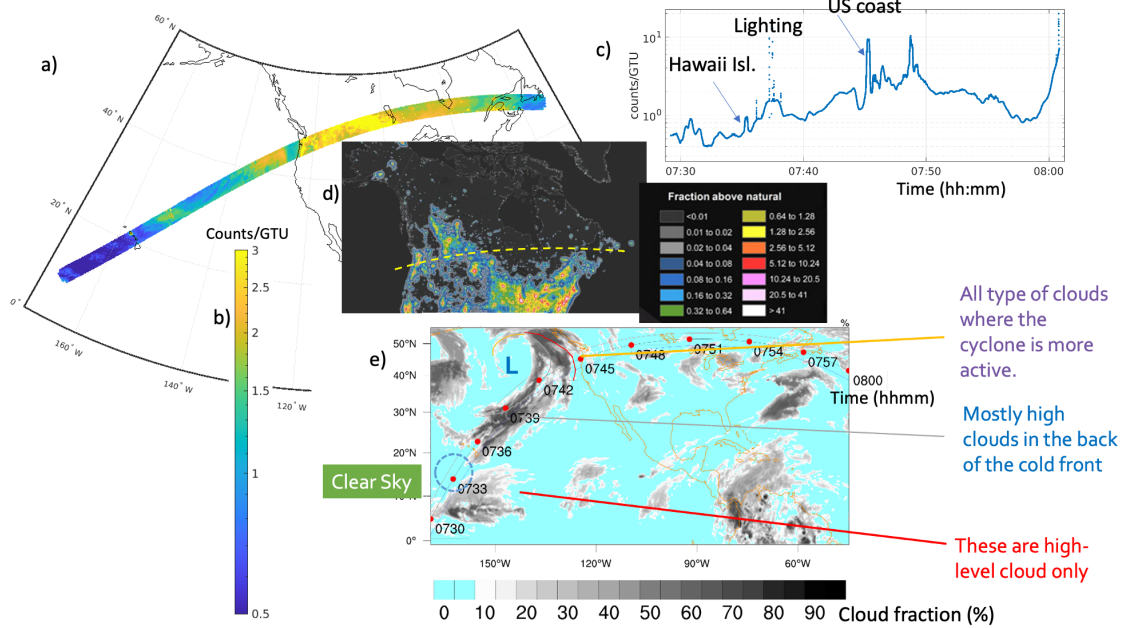

Figure 2: The figure shows a portion of an orbit of Mini-EUSO on Session 30 (January 9th 2021). Image a) shows the UV map of Mini-EUSO as a function of longitude and latitude. The counts/pix/GTU are color-coded in image b). They have been taken in D3 mode but normalized to the D1 GTU. Plot c) displays the light curve along the orbit of one pixel of Mini-EUSO. Plot d) presents the map of artificial lights taken from [15] (with a scale in fraction above natural light intensity), while e) the atmospheric conditions during the passage over ocean by means of a GFS post-processing analysis of the weather forecasts. The orbit of Mini-EUSO is highlighted by the three lines indicating the center and edges of the FoV. See text for details.

conditions, sea and land, various lunar phases are reported in [17]. Assuming no-moon conditions

and typical land/ocean and clear/cloudy atmosphere ratios equal to 30/70, the average background level is ~1.3 counts/pix/GTU, slightly below 1 counts/pix/GTU on ocean and clear sky, while a factor 1.5 - 2 higher in presence of clouds. The average counts on land are ~1.5 times higher than on ocean due to the tail of the distribution associated to the passage over civilized areas. However, deserts and forests have much lower background values, ideal for collecting low energy events.

4. Mini-EUSO duty cycle and exposure

Mini-EUSO data have been utilized to estimate the duty cycle as a function of background light for future space-based UHECR missions, such as the original JEM-EUSO, or the newly proposed M-EUSO mission. Using the complete Mini-EUSO dataset, we counted the number of instances in which each pixel recorded a given background level. Since Mini-EUSO preferably operates under favorable lunar conditions (i.e., near the new Moon, corresponding to lower background levels), we applied a correction to account for this observational bias. Additionally, we evaluated whether the geographical distribution of Mini-EUSO's observations - specifically the time spent over land versus ocean - is representative of a future space-based detector operating continuously. The resulting duty cycle, after applying all the aforementioned correction factors, is presented in Fig. 3.
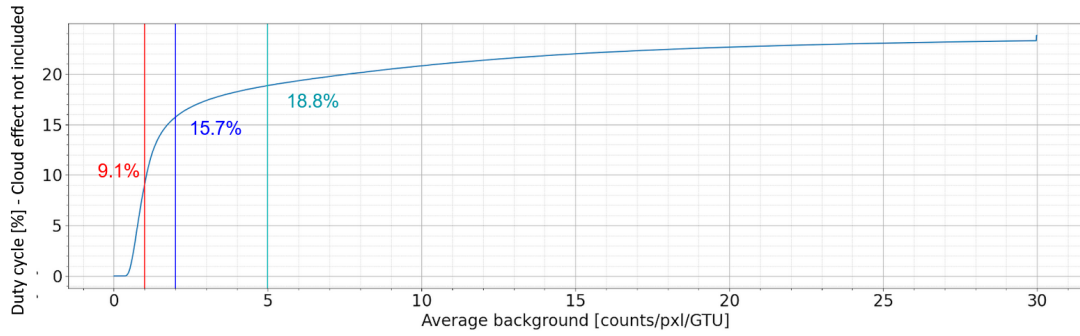

Figure 3: Fraction of time (FoT) a space-based detector would spend below a given background level (BL), accounting for the diurnal and lunar cycles, as well as anthropogenic light sources. The values assume a Mini-EUSO detector efficiency of 8.7%, consistent with that used in ESAF simulations. BLs below 0.4 cts/pix/GTU are never observed, while the last bin integrates the FoT in which it exceeded 30 cts/pix/GTU.

As shown in the figure, approximately 9% (16%) [19%] of the total observation time corresponds to background levels below 1 (2) [5] counts/pixel/GTU. These values incorporate corrections for the day/night cycle, Moon phase, and anthropogenic light sources, but do not account for cloud coverage. It is important to note that the 8.7% detector efficiency assumed here aligns with the value used in ESAF simulations, which were also employed to generate the trigger efficiency curves shown in .1a). These curves represent the trigger performance of Mini-EUSO as a function of energy under varying background conditions, based on ESAF-simulated proton-induced EASs[18]. The curves are obtained either with fixed background conditions of 1 or 2 counts/pix/GTU, or as cumulative distributions. In this second case the cumulative trigger efficiency curve is determined as a weighted sum of each trigger efficiency curve obtained for a specific background level and for the fraction of time in which it occurred. The weighted sum stops at 2 or 5 counts/pix/GTU or extends till 30 counts. The fraction of time in which the measured background by Mini-EUSO is

less than 2(5) counts corresponds to a duty cycle of ~16%(19%). The range of sessions between 20 and 44 have been used to perform this calculation which corresponds to the period in which Mini-EUSO operated in nominal conditions. The fact that both black and green curves tightly enclose the red points obtained at the fixed background level of 1 count/pix/GTU, which was assumed in the pre-flight simulations, confirms the derived duty cycle. This value is very similar to what was considered in the simulations of JEM-EUSO exposure [14]. The effect of clouds is not included yet. In JEM-EUSO a cloud efficiency of $k_c = 0.72$ was estimated. More details on the methodology to derive Mini-EUSO exposure curves and to determine the duty cycle can be found in [19].

The geometrical aperture of Mini-EUSO is obtained by multiplying the footprint of each pixel for 2304 available pixels. Considering the solid angle and the same cloud efficiency k_c of JEM-EUSO, the collected exposure in these 25 sessions corresponds to 1200 Linsley at energies with full efficiency. The projected exposure considering all the data sessions from number 20 to 150 gives a value of ~6500 Linsley. This value is comparable to the one accumulated by ground experiments with hybrid data. Finally, an extrapolation, in the case of continuous operation of Mini-EUSO during the period October 2019 - April 2025 years, leads to a potentially accumulated exposure at the highest energies of ~165,000 Linsley, which is comparable with that collected so far by the surface arrays of Pierre Auger Observatory (PAO) and Telescope Array (TA). These results, despite being obtained with simplified assumptions, provide an idea of the potential of a space-based observatory devoted to the study of UHECRs.

The D1 trigger logic aims at detecting short pulses with time scales comparable to EASs. The most interesting categories of most frequent detected events are Ground Flashers (GFs) and Short Light Transients (SLTs). They are both identified by visually searching for short pulses which are either repeated or not. Sometimes they trigger two consecutive packets and the full shape is visible. Those with a duration ≤ 200 μs were looked at more carefully to check their compatibility with EAS-like events. The visual inspection of the events identified 561 different GFs, some of which with comparable light intensity or event duration of EASs. However, their periodic repetition and a careful comparison with EAS profiles and images on the FS allowed to discriminate them. The same inspection identified 14 SLTs (one of them is shown in Fig. 1b). The origin of those fast flashing lights is still under study, but it seems safe to assume that at least some of them are linked to thunderstorm activity. None of them could be misunderstood with an EAS [20].

5. Preliminary expected performance of M-EUSO based on Mini-EUSO results

The JEM-EUSO collaboration respondend to the recent ESA call for M8 class missions by proposing the M-EUSO payload [2], which consists of a single wide-field UV optical system coupled to two complementary detectors optimized for fluorescence and Cherenkov light, respectively. The key components are a refractive Fresnel lens assembly with 2.3 m diameter ($\gtrsim 4$ m^2 aperture), providing a square-equivalent FoV of ~40°×40° for the fluorescence camera. This corresponds to a pixel angular resolution of 0.12°. The 10 mm-thick lenses will be fabricated from UV-transparent PMMA. The fluorescence camera comprises 49 PDMs based on MAPMTs, with a total of ~112,896 pixels offering single-photon sensitivity. It operates with 2.5 μs sampling for EAS reconstruction and longer integration times (320 μs and 40.96 ms) for complementary science objectives. The Cherenkov camera is mounted at the edge of the FoV and based on silicon photomultipliers

(SiPMs), totaling ~6000 pixels with comparable angular granularity. Operating at 10 ns sampling, it is optimized to detect fast, beamed Cherenkov light from near-horizontal showers directed toward the telescope. These include upward-going EASs from Earth-skimming ν_τ interactions below the limb, as well as highly inclined UHECRs and neutrino-induced EASs skimming the atmosphere just above the limb. An additional compact infrared camera will monitor cloud coverage within and around the main FoV, ensuring accurate exposure determination.

To ensure optimal sky coverage, M-EUSO will operate in low Earth orbit (LEO) at an altitude of approximately 450 km and an inclination of ~30°. This configuration guarantees near-uniform full-sky exposure over the course of the mission, while avoiding the exposure deficits at high declination that affect lower-inclination orbits. M-EUSO will operate in two complementary observational modes to meet its full science goals across the ultra-high-energy regime: a nadir mode for UHECR studies at the lowest possible threshold, and a tilted mode optimized for neutrino detection and for enhancing exposure at the highest energies.

Based on the Mini-EUSO-derived duty cycle the expected annual exposure in nadir mode is ~30,000 km^2 sr yr. This exceeds, in just one year, the total lifetime exposure of TA, and corresponds to 25% of the exposure accumulated by the PAO over 20 years. After this initial phase, M-EUSO will move to tilted mode, pointing toward the Earth's limb. Although the energy threshold increases due to longer light paths and lower photon collection efficiency, the accessible atmospheric volume and geometrical aperture grow substantially. In this configuration, the mission will reach ~100,000 km^2 sr yr per year above 3×10^{20} eV.

M-EUSO's expected performance is based on consolidated simulations using the ESAF framework [18], developed and benchmarked through the design studies of K-EUSO and POEMMA. The fluorescence camera parameters are grounded in actual calibration data from EUSO-SPB2, while background and duty cycle assumptions are derived from in-orbit measurements by Mini-EUSO. M-EUSO is expected to have an energy resolution of ~30(20)% at ~$5\times10^{19}(3\times10^{20})$ eV and an angular one of ~5°(2°) for 60° inclined EAS. These capabilities support robust reconstruction of the UHECR energy spectrum and sky distribution, enabling anisotropy studies and comparisons with nearby extragalactic structure catalogs. The angular resolution is sufficient to search for source correlations above the expected magnetic deflection scale at the highest energies.

6. Acknowledgements

References

[1] A. Coleman et al., *Ultra high energy cosmic rays The intersection of the Cosmic and Energy Frontiers*, *Astroparticle Physics* **149** (2023) 102819 [2205.05845].

[2] J. Eser et al., *From Ground to Space: An Overview of the JEM-EUSO Program for the Study of UHECRs and Astrophysical Neutrinos*, *This Conf. Proceedings* **ICRC2025** (2025) .

[3] G. Abdellaoui et al., *EUSO-TA - First results from a ground-based EUSO telescope*, *Astroparticle Physics* **102** (2018) 98 [1909.09346].

[4] J.H. Adams Jr. et al., *A Review of the EUSO-Balloon Pathfinder for the JEM-EUSO Program*, *Space Science Reviews* **218** (2022) 3.

[5] G. Abdellaoui et al., *Euso-spb1 mission and science*, *Astropa. Phys.* **154** (2024) 102891.

[6] J.H. Adams Jr. et al., *The euso-spb2 fluorescence telescope for the detection of ultra-high energy cosmic rays*, *Astroparticle Physics* **165** (2025) 103046.

[7] J. Eser et al., *POEMMA-Balloon with Radio, towards a space-based Multi-Messenger Observatory*, *PoS(UHECR2024)* **484** (2025) .

[8] P.A. Klimov et al., *The TUS Detector of Extreme Energy Cosmic Rays on Board the Lomonosov Satellite*, *Space Science Reviews* **212** (2017) 1687 [1706.04976].

[9] S. Bacholle et al., *Mini-EUSO Mission to Study Earth UV Emissions on board the ISS*, *Astrophys. J. Suppl.* **253** (2021) 36 [2010.01937].

[10] P.A. Klimov et al., *Status of the K-EUSO Orbital Detector of Ultra-High Energy Cosmic Rays*, *Universe* **8** (2022) 88 [2201.12766].

[11] A. Olinto et al., *The POEMMA (Probe of Extreme Multi-Messenger Astrophysics) observatory*, *JCAP* **2021** (2021) 007 [2012.07945].

[12] M. Battisti et al., *Onboard performance of the level 1 trigger of the mini-EUSO telescope*, *Advances in Space Research* **70** (2022) 2750.

[13] M. Battisti et al., *An end-to-end calibration of the mini-euso detector in space*, *Astroparticle Physics* **165** (2025) 103057.

[14] J.H. Adams Jr. et al., *An evaluation of the exposure in nadir observation of the JEM-EUSO mission*, *Astroparticle Physics* **44** (2013) 76 [1305.2478].

[15] F. Falchi, P. Cinzano, D. Duriscoe, C.C.M. Kyba, C.D. Elvidge, K. Baugh et al., *The new world atlas of artificial night sky brightness*, *Science Advances* **2** (2016) e1600377.

[16] Nat. Cent. for Environ. Pred., Nat. Weather Serv., NOAA, U.S. Dep. of Comm. http://dx.doi.org/10.5065/D65Q4TSG.

[17] M. Casolino et al., *Observation of night-time emissions of the Earth in the near UV range from the ISS with Mini-EUSO*, *Rem. Sens. of Envir.* **284** (2023) 113336 [2212.02353].

[18] S. Abe et al., *Developments and results in the context of the JEM-EUSO program obtained with the ESAF simulation and analysis framework*, *EPJC* **83** (2023) .

[19] M. Bertaina et al., *The Mini-EUSO telescope on board the International Space Station: mission results in view of UHECR measurements from space*, *PoS(UHECR2024)* **484** (2025) .

[20] M. Battisti et al., *Analysis of EAS-like events detected by the Mini-EUSO telescope*, *PoS(ICRC2023)* **444** (2023) .

Full Authors list: The JEM-EUSO Collaboration

M. Abdullahi^{ep,er} M. Abrate^{ek,el}, J.H. Adams Jr.^{ld}, D. Allard^{cb}, P. Alldredge^{ld}, R. Aloisio^{ep,er}, R. Ammendola^{ei}, A. Anastasio^{ef}, L. Anchordoqui^{le}, V. Andreoli^{ek,el}, A. Anzalone^{eh}, E. Arnone^{ek,el}, D. Badoni^{ei,ej}, P. von Ballmoos^{ce}, B. Baret^{cb}, D. Barghini^{ek,em}, M. Battisti^{ei}, R. Bellotti^{ea,eb}, A.A. Belov^{ia,ib}, M. Bertaina^{ek,el}, M. Betts^{lm}, P. Biermann^{da}, F. Bisconti^{ee}, S. Blin-Bondil^{cb}, M. Boezio^{ey,ez} A.N. Bowaire^{ek,el} I. Buckland^{ez}, L. Burmistrov^{ka}, J. Burton^{lc}, F. Cafagna^{ea}, D. Campana^{ef,eu}, F. Capel^{db}, J. Caraca^{lc}, R. Caruso^{ec,ed}, M. Casolino^{ei,ej}, C. Cassardo^{ek,el}, A. Castellina^{ek,em}, K. Černý^{ba}, L. Conti^{en}, A.G. Coretti^{ek,el}, R. Cremonini^{ek,ev}, A. Creusot^{cb}, A. Cummings^{lm}, S. Davarpanah^{ka}, C. De Santis^{ei}, C. de la Taille^{ca}, A. Di Giovanni^{ep,er}, A. Di Salvo^{ek,el}, T. Ebisuzaki^{fc}, J. Eser^{ln}, F. Fenu^{eo}, S. Ferrarese^{ek,el}, G. Filippatos^{lb}, W.W. Finch^{lc}, C. Fornaro^{en}, C. Fuglesang^{ja}, P. Galvez Molina^{lp}, S. Garbolino^{ek}, D. Garg^{li}, D. Gardiol^{ek,em}, G.K. Garipov^{ia}, A. Golzio^{ek,ev}, C. Guépin^{cd}, A. Haungs^{da}, T. Heibges^{lc}, F. Isgrò^{ef,eg}, R. Iuppa^{ew,ex}, E.G. Judd^{la}, F. Kajino^{fb}, L. Kupari^{li}, S.-W. Kim^{ga}, P.A. Klimov^{ia,ib}, I. Kreykenbohm^{dc} J.F. Krizmanic^{lj}, J. Lesrel^{cb}, F. Liberatori^{ej}, H.P. Lima^{ep,er}, D. Mandát^{bb}, M. Manfrin^{ek,el}, A. Marcelli^{ei}, L. Marcelli^{ei}, W. Marszał^{ha}, G. Masciantonio^{ei}, V.Masone^{ef}, J.N. Matthews^{lg}, E. Mayotte^{lc}, A. Meli^{lo}, M. Mese^{ef,eg,eu}, S.S. Meyer^{lb}, M. Mignone^{ek}, M. Miller^{li}, H. Miyamoto^{ek,el}, T. Montaruli^{ka}, J. Moses^{lc}, R. Munini^{ey,ez} C. Nathan^{lj}, A. Neronov^{cb}, R. Nicolaidis^{ew,ex}, T. Nonaka^{fa}, M. Mongelli^{ea}, A. Novikov^{lp}, F. Nozzoli^{ex}, E. M'sihid^{cb}, T. Ogawa^{fc}, S. Ogio^{fa}, H. Ohmori^{fc}, A.V. Olinto^{ln}, Y. Onel^{li}, G. Osteria^{ef,eu}, B. Panico^{ef,eg,eu}, E. Parizot^{cb,cc}, G. Passeggio^{ef}, T. Paul^{ln}, M. Pech^{ba}, K. Penalo Castillo^{le}, F. Perfetto^{ef,eu}, L. Perrone^{es,et}, C. Petta^{ec,ed}, P. Picozza^{ei,ej,fc}, L.W. Piotrowski^{hb}, Z. Plebaniak^{ei}, G. Prévôt^{cb}, M. Przybylak^{hd}, H. Qureshi^{ef,eu}, E. Reali^{ei}, M.H. Reno^{li}, F. Reynaud^{ek,el}, E. Ricci^{ew,ex}, M. Ricci^{ei,ee}, A. Rivetti^{ek}, G. Saccà^{ed}, H. Sagawa^{fa}, O. Saprykin^{ic}, F. Sarazin^{lc}, R.E. Saraev^{ia,ib}, P. Schovánek^{bb}, V. Scotti^{ef,eg,eu}, S.A. Sharakin^{ia}, V. Scherini^{es,et}, H. Schieler^{da}, K. Shinozaki^{ha}, F. Schröder^{lp}, A. Sotgiu^{ei}, R. Sparvoli^{ei,ej}, B. Stillwell^{lb}, J. Szabelski^{hc}, M. Takeda^{fa}, Y. Takizawa^{fc}, S.B. Thomas^{lg}, R.A. Torres Saavedra^{ep,er}, R. Triggiani^{ea}, C. Trimarelli^{ep,er} D.A. Trofimov^{ia}, M. Unger^{da}, T.M. Venters^{lj}, M. Venugopal^{da}, C. Vigorito^{ek,el}, M. Vrabel^{ha}, S. Wada^{fc}, D. Washington^{lm}, A. Weindl^{da}, L. Wiencke^{lc}, J. Wilms^{dc}, S. Wissel^{lm}, I.V. Yashin^{ia}, M.Yu. Zotov^{ia}, P. Zuccon^{ew,ex}.

^{ba} Joint Laboratory of Optics, Faculty of Science, Palacký University, Olomouc, Czech Republic

^{bb} Institute of Physics of the Czech Academy of Sciences, Prague, Czech Republic

^{ca} Omega, Ecole Polytechnique, CNRS/IN2P3, Palaiseau, France

^{cb} Université de Paris, CNRS, AstroParticule et Cosmologie, F-75013 Paris, France

^{cc} Institut Universitaire de France (IUF), France

^{cd} Laboratoire Univers et Particules de Montpellier, Université Montpellier, CNRS/IN2P3, CC72, place Eugène Bataillon, 34095, Montpellier Cedex 5, France

^{ce} IRAP, Université de Toulouse, CNRS, Toulouse, France

^{da} Karlsruhe Institute of Technology (KIT), Germany

^{db} Max Planck Institute for Physics, Munich, Germany

^{dc} University of Erlangen-Nuremberg, Erlangen, Germany

^{ea} Istituto Nazionale di Fisica Nucleare - Sezione di Bari, Italy

^{eb} Università degli Studi di Bari Aldo Moro, Italy

^{ec} Dipartimento di Fisica e Astronomia "Ettore Majorana", Università di Catania, Italy

^{ed} Istituto Nazionale di Fisica Nucleare - Sezione di Catania, Italy

[ee] Istituto Nazionale di Fisica Nucleare - Laboratori Nazionali di Frascati, Italy

[ef] Istituto Nazionale di Fisica Nucleare - Sezione di Napoli, Italy

[eg] Università di Napoli Federico II - Dipartimento di Fisica "Ettore Pancini", Italy

[eh] INAF - Istituto di Astrofisica Spaziale e Fisica Cosmica di Palermo, Italy

[ei] Istituto Nazionale di Fisica Nucleare - Sezione di Roma Tor Vergata, Italy

[ej] Università di Roma Tor Vergata - Dipartimento di Fisica, Roma, Italy

[ek] Istituto Nazionale di Fisica Nucleare - Sezione di Torino, Italy

[el] Dipartimento di Fisica, Università di Torino, Italy

[em] Osservatorio Astrofisico di Torino, Istituto Nazionale di Astrofisica, Italy

[en] Uninettuno University, Rome, Italy

[eo] Agenzia Spaziale Italiana, Via del Politecnico, 00133, Roma, Italy

[ep] Gran Sasso Science Institute, L'Aquila, Italy

[er] INFN, Gran Sasso National Laboratory, Assergi (AQ), I-67100, Italy

[es] University of Salento, via per Arnesano, 73100, Lecce, Italy

[et] INFN Section of Lecce, via per Arnesano, 73100, Lecce, Italy

[eu] Centro Universitario di Monte Sant'Angelo, Via Cintia, 80126 Naples, Italy

[ev] Arpa Piemonte, Via Pio VII, 9 - 10135 Turin

[ew] University of Trento, Via Sommarive 14, 38123 Trento, Italy

[ex] INFN - TIFPA, Via Sommarive 14, 38123 Trento, Italy

[ey] IFPU, Via Beirut, 2, I-34014 Trieste, Italy

[ez] INFN, Sezione di Trieste, Padriciano 99, I-34149 Trieste, Italy

[fa] Institute for Cosmic Ray Research, University of Tokyo, Kashiwa, Japan

[fb] Konan University, Kobe, Japan

[fc] RIKEN, Wako, Japan

[ga] Korea Astronomy and Space Science Institute

[ha] National Centre for Nuclear Research, Otwock, Poland

[hb] Faculty of Physics, University of Warsaw, Poland

[hc] Stefan Batory Academy of Applied Sciences, Skierniewice, Poland

[hd] University of Lodz Doctoral School of Exact and Natural Sciences, 21/23 Jana Matejki Street, 90-237 Łódź, Poland

[ia] Skobeltsyn Institute of Nuclear Physics, Lomonosov Moscow State University, Leninskie gory, 1(2), 119234, Moscow, Russia

[ib] Faculty of Physics, Lomonosov Moscow State University, Leninskie gory, 1(2), 119234, Moscow, Russia

[ic] Space Regatta Consortium, Korolev, Russia

[ja] KTH Royal Institute of Technology, Stockholm, Sweden

[ka] Département de Physique Nucléaire et Corpusculaire, Université de Genève, CH-1211 Genève, Switzerland

[la] Space Science Laboratory, University of California, Berkeley, CA, USA

[lb] University of Chicago, IL, USA

[lc] Colorado School of Mines, Golden, CO, USA

[ld] University of Alabama in Huntsville, Huntsville, AL, USA

[le] Lehman College, City University of New York (CUNY), NY, USA

[lg] University of Utah, Salt Lake City, UT, USA

[li] University of Iowa, Iowa City, IA, USA

[lj] NASA Goddard Space Flight Center, Greenbelt, MD, USA

lm Pennsylvania State University, PA, USA

ln Columbia University, Columbia Astrophysics Laboratory, 538 West 120th Street, New York, NY 10027, USA

lo North Carolina A&T State University, Physics Department, 1601 E Market St, Greensboro, NC 27411, USA

lp University of Delaware, Bartol Research Institute, Department of Physics and Astronomy, Sharp Lab, 104 The Green, Newark, DE 19716, USA